Gasulla Mestre, I.; Kahn, JM. (2015). Performance of Direct-Detection Mode-Group-Division Multiplexing using Fused Fiber Couplers. Journal of Lightwave Technology. 33(9):1748-1760. doi:10.1109/JLT.2015.2392255.

Performance of Direct-Detection Mode-Group-Division Multiplexing using Fused Fiber Couplers

Ivana Gasulla and Joseph M. Kahn, *Fellow, IEEE*

***Abstract*—We present an end-to-end performance evaluation of a mode-group-division multiplexing system that uses direct detection instead of coherent detection, avoiding complex digital signal processing. The system transmits four data channels through a step-index fiber supporting six spatial modes comprising four mode groups, considering the two-fold degeneracy of the LP_{lm} modes for $l \neq 0$. Multiplexing and demultiplexing is performed using two- and three-core fused fiber couplers, each one phase-matched to a group of degenerate modes. These devices are analyzed through a field-based model that describes, for the first time to our knowledge, crosstalk between all the fiber modes. Propagation through the few-mode fiber is modeled considering differential modal attenuation, intermodal dispersion, chromatic dispersion, and both intergroup and intragroup modal coupling. The end-to-end link is described by a concatenation of matrix operators describing the optical field transfer functions for the multiplexer, fiber and demultiplexer. Error-free transmission of four 32-Gb/s OOK-modulated data channels through a 1-km link proves the feasibility of the proposed direct-detection mode-group-division multiplexing approach.**

***Index Terms*—Optical fiber communication, few-mode fibers, mode-group-division multiplexing.**

I. Introduction

SINGLE-MODE fiber (SMF) systems are expected to reach a capacity ceiling of the order of 100 Tb/s [1], owing to the effects of optical amplifier noise, the fiber Kerr nonlinearity, and the limited bandwidth of optical amplifiers. Higher transmission capacities may be achieved by exploiting spatial degrees of freedom [2]. Space-division multiplexing (SDM) may exploit the plurality of cores in multicore fiber (MCF) or the plurality of modes in multimode fiber (MMF). SDM in MMFs can multiplex data signals into individual modes (or near-orthogonal linear combinations of modes), a method called mode-division multiplexing (MDM), or in groups of modes having degenerate (or nearly degenerate) propagation constants, an approach called mode-group-division multiplexing (MGDM).

SDM techniques may be employed in short-reach systems, which typically employ direct detection, or in long-haul systems, which now employ coherent detection. In long-haul SDM systems, MMFs are likely to exhibit significant coupling between modes, which is induced by index imperfections or mechanical stresses. The crosstalk caused by mode coupling can be compensated by coherent detection and multi-input multi-output (MIMO) digital signal processing (DSP), and causes no penalty provided the intermodal coupling is unitary. While the vast majority of reported work on SDM in MMF uses coherent detection and MIMO DSP, the complexity of this approach increases with the number of modes. By contrast, in short-range links, it may be possible to design the system carefully to minimize crosstalk, allowing the system to use direct detection and avoid MIMO DSP. This paper pursues the latter approach, with the goal of reducing cost and power consumption for short-range links in local-area networks, data-center interconnects, or access networks

SDM in multiple spatial modes was firstly proposed using conventional MMFs with core diameters of 50-62.5 μm [3], which pose challenges in mode coupling and crosstalk because of the large number of propagating modes. Subsequently designed few-mode fibers (FMF) supporting a smaller number of modes enable greater control of modal profiles, dispersion and coupling, leading to more stable transmission performance [4,5]. In coherent long-haul systems, the FMF must be optimized to yield a low differential group delay (DGD) between modes, in order to reduce the memory length requirements for MIMO processing. FMF transmission supporting in 12 modes (six spatial modes) was first demonstrated in 2012 [6]. By proper design of a graded-index (GI) profile, the maximum DGD was reduced to 69 ps/km, and a capacity of 480 Gb/s over a 130-km link was achieved. In contrast, previous work on short-distance links has reported FMFs with step-index (SI) profiles optimized to obtain well-differentiated modal propagation constants, thereby minimizing intermodal coupling. Following this approach, Salsi et al. designed a SI FMFs supporting six spatial modes, using a core radius a = 7.5 μm and a large index difference (Δ = 0.97%), to [7]. We follow a similar approach, using SI FMF to minimize coupling between mode groups.

Manuscript received November 9, 2014; revised December 22, 2014; accepted December 30, 2014. Date of publication , 2015; date of current version , 2015. Ivana Gasulla was supported by the Fulbright Commission and the Spanish Ministerio de Educacion through the Programa Nacional de Movilidad de Recursos Humanos del Plan Nacional de I-D+i 2008-2011. Joseph M. Kahn was supported by a Google Faculty Research Award.

Ivana Gasulla is with the Optical and Quantum Communications Group, ITEAM Research Institute, Universitat Politecnica de Valencia, 46022 Valencia, Spain (e-mail: ivgames@iteam.upv.es). Previously, she was with the Edward L. Ginzton Laboratory, Department of Electrical Engineering, Stanford University, Stanford, CA 94305, USA.

Joseph M. Kahn is with the Edward L. Ginzton Laboratory, Department of Electrical Engineering, Stanford University, Stanford, CA 94305, USA (e-mail: jmk@ee.stanford.edu).

The efficient multiplexing/demultiplexing of data signals to/from different spatial modes poses a challenge for MDM or MGDM systems. One common approach uses free-space optics, selecting modes using either fixed selective glass phase masks [4] or programmable Liquid Crystal on Silicon (LCOS) spatial light modulators (SLM) [5],[8,9]. The main disadvantage of free-space optics schemes are high losses, which scale as order $1/N$ at both the multiplexer and demultiplexer, where N is the number of data channels. These losses can be reduced using spot-based couplers that launch spatially separated spots into an FMF, so that each spot maps to a near-orthogonal combination of modes [10]. These spot-based couplers cannot be applied in direct-detection systems, however, since MIMO DSP is required to compensate for crosstalk.

As an alternative to free-space optics, multiplexing/demultiplexing in modes (or mode groups) can be achieved using guided-wave optics, whether in fibers or planar waveguides, which can, in principle, have minimal insertion losses. This approach includes converters based on mechanically induced long-period fiber gratings [11], and recently proposed few-core mode-selective couplers [12-14], which may be fabricated in photonic-crystal technology. Photonic lanterns offer another promising approach based on lossless adiabatic tapers that merge a set of SMFs into a set of MMF modes. Similar to spot-based couplers, the light coming from each SMF couples to an orthogonal combination of modes [15]. This approach does not typically allow modal selectivity, which is required for direct-detection systems, except if different single-mode (SM) cores are used, which may imply incompatibility with circularly symmetric fibers [16].

Guided-wave optics based on silicon photonics have also been considered for MDM, promising low-cost and high-volume manufacturability [17]. However, it is difficult to couple an optical fiber efficiently to the facet of a silicon photonic waveguide, owing to the complex two-dimensional structure of the modes. Various solutions have been published, including one-dimensional grating couplers arranged in a triangular lattice to match the core distribution of a MCF [17] and planar two-dimensional grating couplers driven in anti-phase [18].

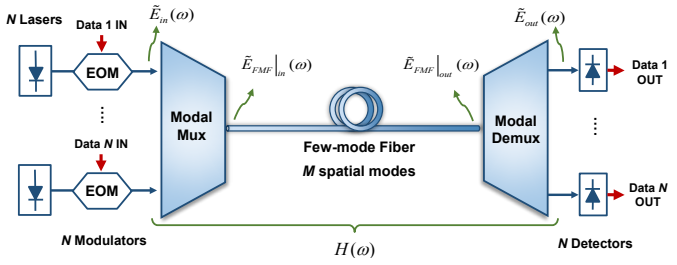

Fig. 1. General scheme for the MGDM end-to-end system.

Considering the simplicity and low losses offered by fused few-core fiber couplers, this paper employs them for multiplexing/demultiplexing in a direct-detection MGDM system. The proposed scheme is depicted in Fig. 1. N independent data signals are transmitted in a fiber supporting M spatial modes, where $N \leq M$. The overall optical link comprising the multiplexer, the M-mode fiber, and the demultiplexer is modeled as a concatenation of matrix operators describing the corresponding optical field transfer functions.

II. Modal Multiplexers and Demultplexers

A. Mode-Selective Couplers

Mode-selective fiber couplers rely on the phase-matching of a higher-order mode in a multimode or few-mode (FM) core with the fundamental mode of a closely positioned SM core. Fig. 2 illustrates a three-core selective coupler proposed by Love and Riesen [12] that is able to decouple or extract both symmetric (LP_{0m}) and asymmetric modes (LP_{lm}) from the FM core (core 1) to a *combination* of both SM cores (cores 2 and 3). Using this configuration, all asymmetric field modes can be recovered, even when they lie at a random orientation angle α with respect to the horizontal axis, as defined in Fig. 2.

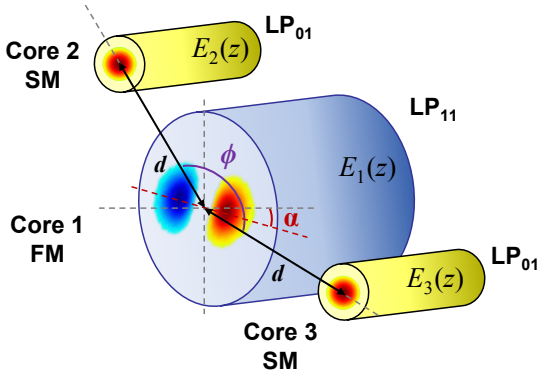

Fig. 2. Individual mode-selective coupler. SM: single-mode, FM: few-mode.

Although the analytical model presented by Love and Riesen shows the potential of the three-core coupler for decoupling individual modes, it does not address the problem of a realistic mode-division multiplexing system where not only one, but a whole set of higher-order modes propagates through the FMF. It is thus desirable to derive a general model that considers any phase-matching condition between the modes propagating through the different cores, i.e., $\Delta\beta = \beta_1 - \beta_{2,3} \neq 0$, (where β_i is the propagation constant of the electric field propagating through core i), so the performance of the coupler can be evaluated for both the desired and interfering modes. This is a strict requirement for the proper design of a complete multiplexer or demultiplexer device.

The electric field e_i (r,ϕ,z) for a given mode in core $i = \{1,2,3\}$, assumed propagating along the positive z direction, can be expressed in cylindrical coordinates as

$$e_i(r,\phi,z) = E_i(z)\, e^{-j\omega t}\, f_i(r,\phi), \tag{1}$$

where $E_i(z)$ is the modal complex amplitude, ω the optical angular frequency and $f_i(r,\phi)$ the modal spatial distribution.

The interaction between co-propagating fields the cores can be described by the coupled-mode equations:

$$\begin{pmatrix} dE_1(z)/dz \\ dE_2(z)/dz \\ dE_3(z)/dz \end{pmatrix} = \begin{pmatrix} -j\beta_1 & jC_2 & jC_3 \\ jC_2 & -j\beta_2 & 0 \\ jC_3 & 0 & -j\beta_3 \end{pmatrix} \begin{pmatrix} E_1(z) \\ E_2(z) \\ E_3(z) \end{pmatrix}, \quad (2)$$

where β_i is the propagation constant of the modal field propagating through core i, C_2 and C_3 are the coupling coefficients between cores 1 and, respectively cores 2 and 3. Note that, as in [12], no coupling between both outer cores 2 and 3 is considered. In addition, given the short length of core 1 within the selective coupler (usually less than 1 cm), intermodal coupling can be considered negligible.

Assuming weak guidance of the electric field within each core, we can approximate the modal distribution $f_i(r,\phi)$ as a linearly polarized fiber mode LP_{lm}, which is defined as:

$$\begin{aligned} f_i(r,\phi) &= A_l \frac{J_l(u_i r/a_i)}{J_l(u_i)}\cos(l\phi) \quad , 0 < r \le a_i \\ f_i(r,\phi) &= A_l \frac{K_l(w_i r/a_i)}{K_l(w_i)}\cos(l\phi) \quad , r > a_i \end{aligned} \quad (3)$$

where J_l is the Bessel function of first kind, K_l is the modified Bessel function of the second kind, l is the azimuthal mode number, as well as u_i, w_i and a_i are, respectively, the core modal index, the cladding modal index and the core radius relative to the i-th core.

Assuming the propagation constant for the fundamental LP_{01} mode is the same in both outer SM, $\beta_2=\beta_3$, the system (2) can be solved analytically by diagonalization to obtain the electrical fields along each core. In particular, we are interested in the expressions for the field transfer functions between input and output of the few-mode fiber (core 1) as well as between this core and both SMFs (cores 2 and 3):

$$H_{Co_1\leftarrow Co_1}(z) = e^{-j\frac{(\beta_1+\beta_2)z}{2}}\left[\cos(\hat{C}z) - j\frac{\Delta\beta}{2\hat{C}}\sin(\hat{C}z)\right], \quad (4)$$

$$H_{Co_2\leftarrow Co_1}(z) = j\frac{C_2}{\hat{C}}e^{-j\frac{(\beta_1+\beta_2)z}{2}}\sin(\hat{C}z) = H_{Co_1\leftarrow Co_2}(z), \quad (5)$$

$$H_{Co_3\leftarrow Co_1}(z) = j\frac{C_3}{\hat{C}}e^{-j\frac{(\beta_1+\beta_2)z}{2}}\sin(\hat{C}z) = H_{Co_1\leftarrow Co_3}(z), \quad (6)$$

where the subindices $Co_i \leftarrow Co_j$ indicate energy transfer from core j to core i and $\hat{C}$ is defined as

$$\hat{C}^2 = \left(\frac{\Delta\beta}{2}\right)^2 + C_2^2 + C_3^2. \quad (7)$$

These transfer functions can describe both multiplexing and demultiplexing operations. We see that the optical field is decoupled from the FM core to each SM core (demultiplexing) or from one/two SM core(s) to the FM core (multiplexing) depending on the phase mismatch $\Delta\beta$ described in the parameter $\hat{C}$.

The coupling coefficients between the FM core and the SM cores (j = 2,3) are given by overlap integrals of the two modal spatial distributions involved over the FM core area:

$$C_j = \frac{\omega}{2}\int_{\phi_1=0}^{2\pi}\int_{r_1=0}^{a_1}\varepsilon_0(n_{co,1}^2 - n_{cl}^2)f_j(r_j,\phi_j)f_1(r_1,\phi_1)dr_1 d\phi_1 \ , \quad (8)$$

where (r_1, ϕ_1) are coordinates in core 1, ε_0 is the vacuum permittivity, $n_{co,1}$ is the refractive index of core 1 and n_{cl} is the refractive index of the cladding.

For the particular design where both SM cores are identical and their centers (see Fig. 2) are separated by the optimum angle $\Phi = \pi/(2l_{match}) + n\pi/l_{match}$, for n = {0,1,2, …} and l_{match} being the azimuthal number of the mode matched to the coupler, all the power of the matched mode can be decoupled to the two cores [12]. In other words, for the optimum selection of the coupler length [19], which allows us to maximize/minimize the transfer function $H_{Coi\leftarrow Coj}$, all the power of an asymmetric matched mode LP_{lm} mode can be decoupled regardless the modulus and phase of both degenerate modes involved, i.e., for any complex weights x_a and x_b so that $LP_{lm} = x_a LP_{lma} + x_b LP_{lmb}$.

Since weak guidance is assumed, and for the optimum Φ angle, the field coupling coefficients can be derived from (8) as

$$C_2 = -\frac{C_{R,2}}{\sqrt{2}} \text{ and } C_3 = -\frac{C_{R,3}}{\sqrt{2}} \quad \text{for } LP_{0m} \ , \quad (9)$$

$$C_2 = -C_{R,2}\cos\left(\frac{l}{l_{match}}\frac{\pi}{2}\right) \text{ and } C_3 = -C_{R,3} \quad \text{for } LP_{lma} \ , \quad (10)$$

$$C_2 = -C_{R,2}\sin\left(\frac{l}{l_{match}}\frac{\pi}{2}\right) \text{ and } C_3 = 0 \quad \text{for } LP_{lmb} \ , \quad (11)$$

where l is the azimuthal mode number of the asymmetric mode under consideration and $C_{R,i}$ stands for the radial dependence of C_i, (i = 2,3). We can see that for the particular design where both SM cores are identical ($C_{R,2} = C_{R,3} = C_R$), the energy from a symmetric mode LP_{0m} is equally decoupled to both SM cores. The energy from a group of degenerated modes (asymmetric LP_{lm}) that is matched to the coupler ($l = l_{match}$) is distributed so that the energy of LP_{lma} (α = 0) goes *entirely* to core 3 while LP_{lmb} ($\alpha = \pi/(2l)$) decouples *entirely* to core 2. On the other hand, the crosstalk coming from a group of degenerate modes that is not matched to the coupler depends on the ratio l/l_{match} and the radial dependence $C_{R,i}$, which is a function of the properties of the decoupled group of degenerate modes as well as the coupler design. It is calculated following a procedure similar to that in [13]:

$$C_{R,i} = (-1)^l \frac{2\sqrt{2}ka_1\Delta_1 u_1 u_i n_{co,1}^{3/2}}{a_i v_1 v_i n_{co,i}^{1/2}} \cdot \frac{K_l(w_i d/a_i)}{K_1(w_i)\sqrt{K_{l-1}(w_1)K_{l+1}(w_1)}} \cdot \frac{\left[w_i' I_{l+1}(w_i')K_l(w_1) + w_1 I_l(w_i')K_{l+1}(w_1)\right]}{w_i'^2 + u_1^2} \ , \quad (12)$$

where k is the wave-number, $w_i' = w_i a_1/a_i$, d the separation between core 1 and either SM core axis, Δ_1 the relative index difference of core 1 $\Delta_1 = (n_{co,1}^2 - n_{cl}^2)/(2n_{co,1}^2)$, and v_i the normalized frequency of the i-th core $v_i = a_i k(n_{co,1}^2 - n_{cl}^2)^{1/2}$.

The performance of the selective coupler operated as a demultiplexer has been analyzed for the cases where it is matched to each one of the four groups of degenerate modes, [LP_{01}, LP_{11}, LP_{21}, LP_{02}], propagating through a SI FMF characterized by a_1 = 6.48 µm, $n_{co,1}$ = 1.4546 and Δ = 0.685%. The characteristics of each coupler for an optical wavelength of λ_0 = 1550 nm are detailed in Table I. The separation between cores is d = 15 µm. The SM cores use the same refractive index profile ($n_{co,1}$ and Δ) as the FM core, varying the core radius so the phase-matching condition is achieved for each of the matched group of modes. An exception is found in the two-core coupler matched to the LP_{01} mode since, obviously, the refractive index of the SM core must change in order to match the propagation constant of the LP_{01} mode propagating through the FMF, while ensuring SM condition. An alternative for injecting/extracting the fundamental mode would be to omit the coupler and just butt couple the light coming from a standard SMF into the FMF, but this will cause crosstalk from higher-order modes (mainly the LP_{11} modal group) and loss due to the mismatch between the core radii.

TABLE I. CHARACTERISTICS OF SELECTIVE COUPLERS

	Mode matched to the selective coupler			
	LP_{01}	LP_{11}	LP_{21}	LP_{02}
No. cores	2	3	3	2
***a* (µm)**	2.83	3.457	1.991	1.696
Δ	$10.35\cdot10^{-3}$	$6.85\cdot10^{-3}$	$6.85\cdot10^{-3}$	$6.85\cdot10^{-3}$
Φ (rad)	-	π/2	π/4	-
z_c (mm)	57.355	8.084	4.518	3.289

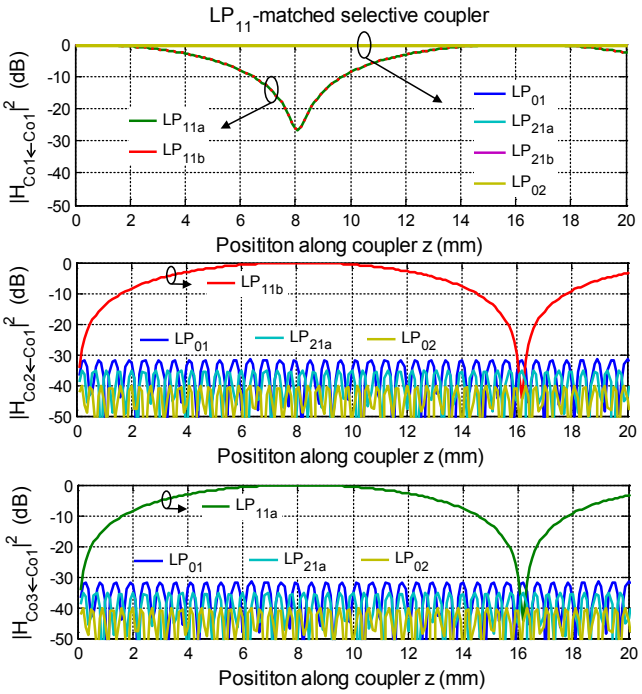

Fig. 3. Magnitude of the transfer function along the coupler length for each core of a three-core coupler matched to the LP_{11} group of modes.

The computed transfer functions of a three-core coupler acting as a demultiplexer, $H_{Coi\leftarrow Co1}$ for cores i = {1,2,3}, [equations (4)-(6)], are plotted in Figs. 3 and 4 versus the position along the coupler z, respectively, for a LP_{11}-matched and a LP_{21}-matched coupler. We observe in both figures that the matched group of modes is decoupled from core 1 to either core 2 (LP_{lmb}) or 3 (LP_{lma}) for a specific coupler length given by $z_c = \pi(2n+1)/(2\hat{C})$ for n = {0,1,2,…}, as deduced from (4)-(6) and specified in Table I. While the level of modal coupling is almost negligible for the LP_{11}-matched coupler, (maximum of -31 dB coming from the LP_{02} mode), it increases to a maximum of -16 dB for the LP_{21}-matched coupler as a consequence of the similarity in the value of the propagation constant of the LP_{21} and LP_{02} modal groups. Evaluation of the multiplexer/ demultiplexer devices as a whole, as well as simulation of end-to-end data transmission, will demonstrate that this crosstalk does not prevent acceptable MGDM system performance.

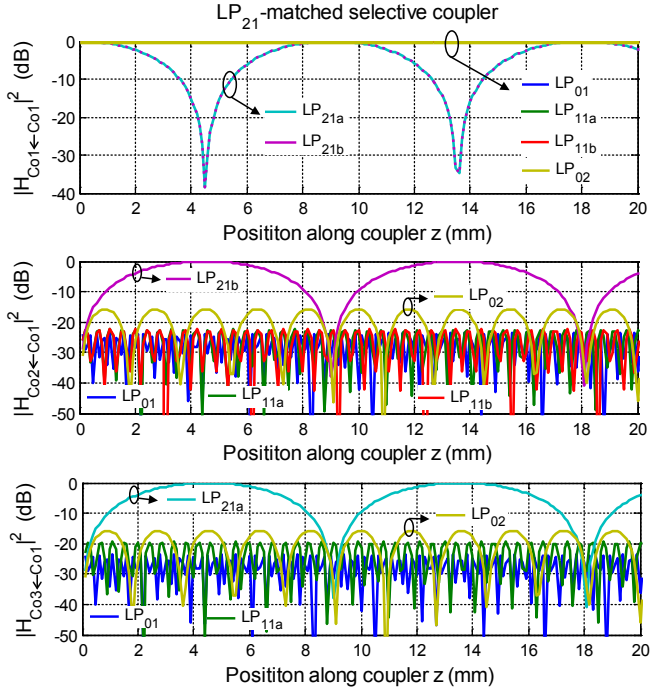

Fig. 4. Magnitude of the transfer function along the coupler length for each core of a three-core coupler matched to the LP_{21} group of modes.

Since the selective mode couplers rely on phase-matching conditions, it is expected that the response of a coupler specifically designed for matching a group of modes at a given optical wavelength will change if the wavelength is varied. To evaluate this behavior, we have computed the transfer function of the selective couplers whose design characteristics are shown in Table I for the entire range of wavelengths (within the standard ITU C band) in which the outer cores remain SM. For instance, the coupler matched to the LP_{11} group of modes maintains SM operation in cores 2 and 3 for the wavelength range between 1547 and 1563 nm. Fig. 5 plots the variation of the transfer function along the central core of this coupler, i.e. $H_{Co1\leftarrow Co1}|_{LP_{11}}$, when varying the input wavelength in 1-nm steps within that band.

The free spectral range of the periodic response is reduced as the wavelength is increased, so the notch that corresponds

to the optimum decoupling from the central to the outer cores moves toward the left along the coupler length. This reduces the coupling efficiency of the matched group by up to 10 dB from its optimum value at 1550 nm, approximately decreasing 1 dB for each 1-nm detuning step. In view of this, we can state that using these fused fiber couplers to WDM + SDM multiplexing architectures is possible if the optical wavelength for which each coupler is matched is kept fixed, i.e. for fixed WDM operation. If WDM with tunable transmitters is required, an alternative solution is to exploit the tapered couplers recently proposed in [20].

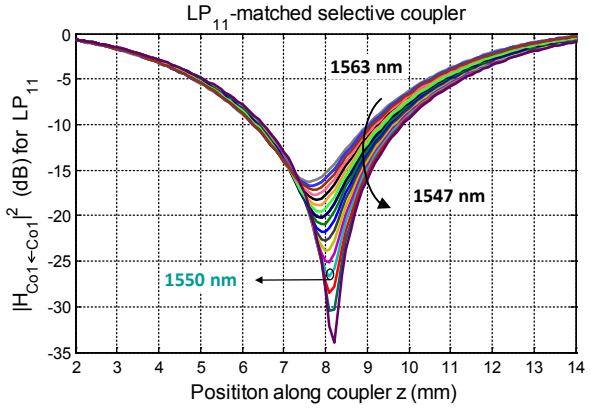

Fig. 5. Variation of the magnitude of the transfer function for the LP_{11} group working in the wavelengths range [1563,1547] nm along the length of core 1 in a coupler matched to the LP_{11} group.

Our extension of the coupled-mode analytical model allows evaluation of phase-matching conditions for any spatial mode propagating through the fiber. This allows a system designer to individually characterize the power penalties and crosstalk interference associated to each one of the selective couplers. Secondly, it serves as a valuable tool to design, for the first time to our knowledge, an entire multiplexer or demultiplexer device implemented through a serial concatenation of single two- or three-core couplers.

B. Modal Multiplexer

We can describe a modal multiplexer by a matrix whose elements are the field transfer functions between individual output spatial modes and input data channels. For our particular MGDM system, where four input data channels are transmitted through a six-spatial-mode fiber, the multiplexer transfer function $H_{MUX}(\omega)$ is described by a 6×4 matrix, so the optical field array at the input of the FMF $\tilde{E}_{FMF}|_{in}(\omega) = H_{MUX}(\omega)\cdot\tilde{E}_{in}(\omega)$, being $\tilde{E}_{in}(\omega)$ the optical field array at the input of the modal multiplexer, as labeled in Fig. 1. Since only a mode belonging to a pair of degenerate modes is excited (LP_{11a} and LP_{21a} in our case), the matrix rows relative to the counterpart LP_{11b} and LP_{21b} modes are set to zero. These modes will be excited once the optical signal is propagated through the FMF as a consequence of the strong random coupling occurring between the pairs of degenerate modes. An MDM scheme in which all spatial modes are used as individual channels will require a 6×6 (generally speaking M×M) matrix where the LP_{11b} and LP_{21b} are also excited in the multiplexer.

Since we decided to transmit data in the specified groups of degenerate modes, the whole modal multiplexer device is designed as a linear sequence of two-core couplers, as proposed in [12] and depicted in Fig. 6, so its overall transfer function $H_{MUX}(\omega)$ results from the concatenation of the transfer functions describing the constituent mode-selective couplers, given by (4)-(6). Each column $H_{MUX}(:,k)$ corresponds to a different input data channel k, resulting in

$$\begin{aligned} H_{MUX}(:,1) &= H_{Co_1\leftarrow Co_2}\big|_{LP01} H_{Co_1\leftarrow Co_1}\big|_{LP11} H_{Co_1\leftarrow Co_1}\big|_{LP21} H_{Co_1\leftarrow Co_1}\big|_{LP02} \\ H_{MUX}(:,2) &= H_{Co_1\leftarrow Co_2}\big|_{LP11} H_{Co_1\leftarrow Co_1}\big|_{LP21} H_{Co_1\leftarrow Co_1}\big|_{LP02} \\ H_{MUX}(:,3) &= H_{Co_1\leftarrow Co_2}\big|_{LP11} H_{Co_1\leftarrow Co_1}\big|_{LP02} \\ H_{MUX}(:,4) &= H_{Co_1\leftarrow Co_2}\big|_{LP02} \end{aligned} \quad , \quad (13)$$

where $H_{Coi\leftarrow Coj}\,|_{LP_{lm}}$ represents the transfer function for the individual coupler matched to the LP_{lm} group of modes.

By contrast, a multiplexer for MDM would comprise a concatenation of two-core and three-core selective couplers, similar to the demultiplexer proposed later in this paper.

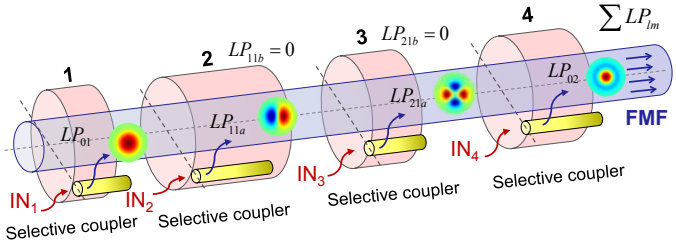

Fig. 6. Multiplexer device as a sequence of two-core couplers.

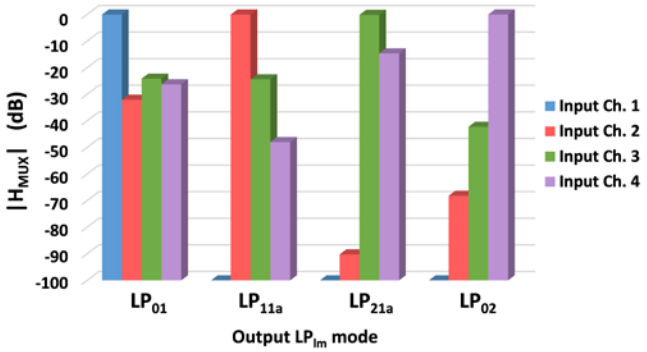

Fig. 7. Modulus of the field transfer function of the multiplexer device.

Fig. 7 illustrates the modulus of the simulated optical transfer function of the multiplexer for each of the four input data channels. We observe for each output LP_{lm} mode (group of bars) a low level of insertion loss for every respective matched input channel (Input Ch. 1 for LP_{01}, Input Ch. 2 for LP_{11a}, Input Ch. 3 for LP_{21a}, and Input Ch. 4 for LP_{02}). This low loss represents an essential advantage over multiplexers implemented using free-space optics. In addition, we observe a non-negligible level of crosstalk (around -16 dB) in the output mode LP_{21a} coming from the input channel 4 as a consequence of the undesired excitation of LP_{21a} in the coupler matched to the LP_{02} mode (coupler 4 in Fig. 6). This is due to the difference in the propagation constants between these two

groups of modes being much smaller than between the rest. The propagation constants computed using our numerical mode solver are [$\beta_{LP_{01}}$ = 5.8887, $\beta_{LP_{11}}$ = 5.8773, $\beta_{LP_{21}}$ = 5.8631, $\beta_{LP_{02}}$ = 5.8597] · 10^6 rad/m at an optical wavelength of 1550 nm. An alternative is to consider both LP_{21} and LP_{02} as being part of the same group of modes, which implies a decrease in the multiplexing efficiency, as the number of channels will be reduced. Nevertheless, we consider them as independent channels. Fig. 7 shows that this level of crosstalk is not symmetric when compared to the approximate -42 dB of crosstalk in the output mode LP_{02} caused by the input channel 3, which is due by the undesired excitation of LP_{02} in the third coupler. This asymmetry results from the fact that the fraction of LP_{02} excited in the third coupler is highly attenuated by $H_{Co1\leftarrow Co1}\,|_{LP_{02}}$ when passing through the following individual coupler (coupler 4 in Fig. 6), which is matched to the LP_{02} mode.

C. Modal Demultiplexer

Fig. 8 shows the schematic of the device for demultiplexing the four data channels from the six spatial modes received from the FMF. In this case, the demultiplexer contains two two-core couplers for the symmetric modes and two three-core couplers to extract the asymmetric modes. We found that in order to minimize crosstalk between the groups of modes with smaller $\Delta\beta$ (LP_{21} and LP_{02}), the cascade of selective couplers for demultiplexing should follow the sequence [LP_{02} → LP_{21}→ LP_{11}→ LP_{01}], as opposed to the sequence selected for multiplexing. Similarly to the multiplexer, the demultiplexer is characterized by a 4×6 matrix H_{DEMUX} that describes the field transfer function connecting the four output channels to the six incoming spatial modes. In this case, each column $H_{DEMUX}(:,k)$ corresponding to a different coupler SM core and, thus, to a different input spatial mode k, is given by

$$
\begin{aligned}
H_{DEMUX}(:,1) &= H_{Co_1\leftarrow Co_2}\big|_{\mathrm{LP02}} \\
H_{DEMUX}(:,2) &= H_{Co_1\leftarrow Co_1}\big|_{\mathrm{LP02}}\, H_{Co_2\leftarrow Co_1}\big|_{\mathrm{LP21}} \\
H_{DEMUX}(:,3) &= H_{Co_1\leftarrow Co_1}\big|_{\mathrm{LP02}}\, H_{Co_3\leftarrow Co_1}\big|_{\mathrm{LP21}} \\
H_{DEMUX}(:,4) &= H_{Co_1\leftarrow Co_1}\big|_{\mathrm{LP02}}\, H_{Co_1\leftarrow Co_1}\big|_{\mathrm{LP21}}\, H_{Co_2\leftarrow Co_1}\big|_{\mathrm{LP11}} \\
H_{DEMUX}(:,4) &= H_{Co_1\leftarrow Co_1}\big|_{\mathrm{LP02}}\, H_{Co_1\leftarrow Co_1}\big|_{\mathrm{LP21}}\, H_{Co_3\leftarrow Co_1}\big|_{\mathrm{LP11}} \\
H_{DEMUX}(:,6) &= H_{Co_1\leftarrow Co_1}\big|_{\mathrm{LP02}}\, H_{Co_1\leftarrow Co_1}\big|_{\mathrm{LP21}}\, H_{Co_1\leftarrow Co_1}\big|_{\mathrm{LP11}}\, H_{Co_2\leftarrow Co_1}\big|_{\mathrm{LP01}}
\end{aligned}
\quad , \quad (14)
$$

where the second and fourth columns relate to the LP_{lma} modes, whereas the third and fifth columns relate to the LP_{lmb} modes.

Special consideration must be given to the groups of degenerate modes, whose decoupled optical signals must be combined at the three-core coupler output in order to extract all the signal energy originally launched into the LP_{11a} and LP_{21a} modes at the multiplexer. As a consequence, we must include an optical or electrical diversity combiner stage before or after photodetection, respectively, to combine the energy received in the two outer SM cores.

Since the three-core transfer function describing the conversion from the horizontally oriented spatial modes, LP_{11a} or LP_{21a}, to the fundamental mode, (i.e., from the FMF to the SM core 3), is the same as that for the vertically oriented spatial modes, LP_{11b} or LP_{21b}, to the fundamental mode, (i.e., from the FMF to the SM core 2):

$$
H_{Co_3\leftarrow Co_1}(z)\big|_{LP_{11a}} = H_{Co_2\leftarrow Co_1}(z)\big|_{LP_{11b}} = -j\frac{C_R}{\hat{C}}e^{-j\frac{(\beta_1+\beta_2)z}{2}}\sin(\hat{C}z), \quad (15)
$$

the constructive or destructive character of the interference resulting from combining both degenerate fields together is a consequence of the phase and amplitude transformation experienced through the fiber propagation, which is described by the FMF random transfer function $H_f(\omega)$.

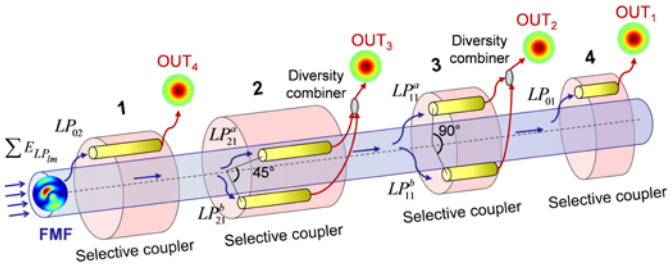

Fig. 8. Demultiplexer device as a sequence of two- and three-core couplers.

We consider electrical diversity combining using three different techniques: best selection combining (BSC), equal-gain combining (EGC) and maximal ratio combining (MRC) [21]. It should be noted that, since no optical inline amplifiers are included, our MGDM system is thermal noise-limited. In BSC, the combiner outputs the signal on the SM core with the highest signal-to-noise ratio, so that the output from the combiner yields a total electrical signal-to-noise ratio (SNR_{tot}) equal to the maximum SNR_i of the branch i ($i = a$ for the spatial mode LP_{lma} and $i = b$ for the spatial mode LP_{lmb}):

$$
SNR_{tot} = SNR_i = \frac{P_i^2}{\sigma^2} \;\rightarrow\; SNR_{tot}\big|_{\mathrm{worst}} = \frac{(P_{tot}/2)^2}{\sigma^2}, \quad (16)
$$

where P_i is the optical power of the selected core output and σ^2 is the noise variance (here, we assume unit photodetector responsivity for simplicity). In a worst-case scenario, i.e. when $P_i = P_{tot}/2$, the SNR, denoted by $SNR_{tot}|_{worst}$, is subject to a 6-dB penalty, which corresponds to a 3-dB optical power penalty. EGC, on the other hand, adds both core outputs with equal weighting, so that SNR_{tot} is subject to a fixed penalty of 3 dB (1.5-dB optical power penalty):

$$
SNR_{tot} = \frac{(P_a+P_b)^2}{2\sigma^2} = \frac{P_{tot}^{\,2}}{2\sigma^2}. \quad (17)
$$

Unlike the previous techniques, in MRC the output is an optimized weighted combination of both output paths. The weights c_i to be applied must be selected in order to maximize the resulting SNR_{tot}. For the selected values of $c_i^{\,2} = P_i^2/\sigma^2$, SNR_{tot} is the sum of both SNR_i:

$$SNR_{tot} = \frac{\left(P_a c_a + P_b c_b\right)^2}{\sigma^2\left(c_a{}^2 + c_b{}^2\right)} = \frac{P_a{}^2 + P_b{}^2}{\sigma^2} \rightarrow SNR_{tot}\big|_{worst} = \frac{P_{tot}{}^2}{2\sigma^2}, \quad (18)$$

which implies an SNR penalty of 3 dB (1.5-dB optical power penalty) for the worst-case scenario.

Implementing optical combining requires applying adaptive co-phasing of one or both outputs before adding them together in a 3-dB coupler in order to obtain the maximum photodetected power. Although this configuration requires only one photodetector and avoids the need for electrical signal processing (in contrast with MRC), it increases optical demultiplexing complexity. One possible approach is the endless phase shifter proposed recently by C. Doerr [22] in the context of an optical MIMO demultiplexer using photonic integration. The so-called endless phase shifter comprises not only a 4π-range phase shifter but also two 1×2 Mach-Zehnder switches such that the overall structure is able to track mode coupling variations occurring in the fiber without interrupting signal reception. A valley-search algorithm is proposed in [22] for control of the phase shifter through the minimization of the output interference RF power. The electrical signal-to-noise ratio of the photodetected signal when adaptive co-phasing yields the maximum photodetected power is given by:

$$SNR_{tot} = \frac{P_{tot}{}^2}{\sigma^2}. \quad (19)$$

A different diversity combiner would need to be applied if MDM were implemented instead of MGDM. Since the degenerate modes would convey different data signals, it would be required to perform optical MIMO processing at the output of the three-core coupler to invert the FMF propagation matrix.

Assuming the combiner has been properly optimized, the absolute value of the demultiplexer field transfer function for each combination of input/output is shown in Fig. 9. As stated for the multiplexer, no loss is introduced by the proposed concatenation of selective couplers, with the exception of the 3-dB penalty associated to the 2×1 combiner required for outputs 2 and 3. In summary, the multiplexer and demultiplexer described in this section demonstrate losses much lower than for devices implemented in free-space optics [5], [8,9]. Our concern continues to be the crosstalk occurring between the mode LP_{21} and the output channel 4 (matched to the LP_{02} mode), in this case happening in the first individual coupler of Fig. 8, which has an approximate level of -16 dB. The same asymmetry explained above for the multiplexer applies here when comparing to the low crosstalk introduced by the mode LP_{02} into the output channel 3 (matched to the LP_{21} mode).

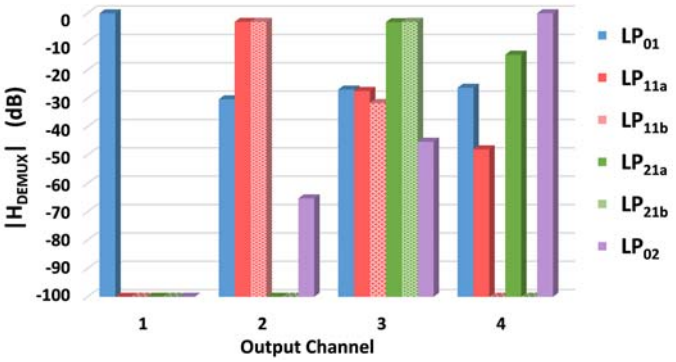

Fig. 9. Modulus of the field transfer function of the demultiplexer device.

Another possibility for the implementation of the whole multiplexer/demultiplexer is to use a single few-core coupler for simultaneously processing all the groups of modes, instead of the cascades of two- and three-core couplers described above. This approach has been reported for the first time in [14] regarding a four-core coupler that works simultaneously with LP_{11} and LP_{21} groups of modes, where its performance is evaluated for the presence of only a single mode group. A more complete analysis of its multiplexing performance would require modeling the intermodal crosstalk associated with the presence of all the mode groups propagating through the FMF, which has not been attempted before. Furthermore, these devices are limited to a low number of groups of modes because of coupling between the outer cores.

III. Few-Mode Fiber

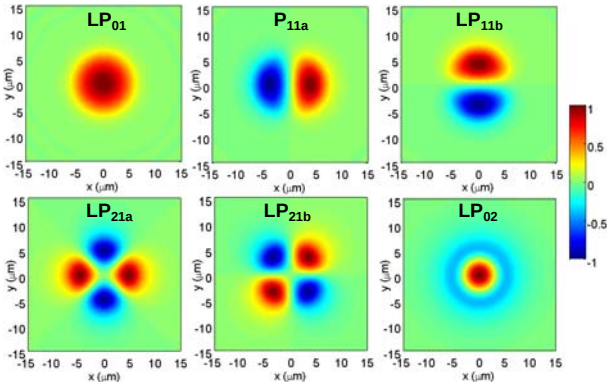

Fig. 10. Normalized spatial profiles of the propagating modal fields.

After numerically evaluating different few-mode fiber solutions considering different step and graded refractive index profiles and the inclusion of trench-assisted configurations around the core, we concluded that an optimal FMF for our MGDM approach employs an SI profile with a radius a_1 = 6.48 μm, a core refractive index $n_{co,1}$ = 1.4546 and a relative index difference $\Delta_1 = 6.85\times10^{-3}$. As pointed out in the previous section, this FMF propagates six spatial modes at a 1550-nm wavelength, whose normalized spatial field profiles are illustrated in Fig. 10. The normalized frequency V is chosen so that the next higher-order mode to be excited is just below cut-off, maximizing confinement of the propagating modes. These modes are considered in this work as four groups of degenerate modes that are used as four

independent transmission channels. The FMF optical transfer function $H_f(\omega)$, described through a 6×6 matrix, accounts for both uncoupled and coupled propagation effects. Our model thus includes differential modal attenuation, modal dispersion, chromatic dispersion and modal coupling, differentiating between intragroup modal coupling (strong coupling between degenerate modes within the same group) and intergroup modal coupling (low or medium coupling between mode groups).

Assuming that M modes propagate along the fiber, the field coupled mode propagation equations in the frequency domain can be expressed as [23,24]:

$$\frac{d\tilde{E}_{FMF}(\omega,z)}{dz} = A(\omega,z)\,\tilde{E}_{FMF}(\omega,z), \tag{20}$$

where $\tilde{E}_{FMF}(\omega,z)$ is a vector containing the M field modes and the elements of the matrix operator $A(\omega,z)$ are given by

$$A_{\mu\nu} = \begin{cases} -\Gamma_\mu(\omega) = -\alpha_\mu(\omega) - j\beta_\mu(\omega), & \mu = \nu \\ \hat{K}_{\mu\nu} f(z), & \mu \neq \nu \end{cases}, \tag{21}$$

where $\alpha_\mu(\omega)$ is the attenuation of the μ-th mode, which is considered independent of ω around the central angular frequency of the light source ω_0, $\alpha_\mu(\omega) \approx \alpha_\mu(\omega_0) = \alpha_\mu{}^0$, $\beta_\mu(\omega)$ is the propagation constant expanded in a second-order Taylor series around ω_0 as

$$\beta_\mu(\omega) = \beta_\mu^0 + \beta_\mu^1(\omega-\omega_0) + \frac{\beta_\mu^2}{2}(\omega-\omega_0)^2 \tag{22}$$

and $K_{\mu\nu} = \hat{K}_{\mu\nu} f(z)$ is the field coupling factor between modes μ and ν, where $f(z)$ describes the actual geometric shape of the core boundary [25].

The field transfer function matrix $H_f(\omega)$ that satisfies

$$\tilde{E}_{FMF}(\omega,z) = H_f(\omega)\tilde{E}_{FMF}(\omega,0) \tag{23}$$

at a given position z can be calculated form (19) as

$$H_f(\omega) = \exp\left[\int_0^z A(\omega,z')dz'\right] = \sum_{l=0}^{\infty} \frac{\left[\int_0^z A(\omega,z')dz'\right]^l}{l!}. \tag{24}$$

From now on, the description of the transfer function matrix will distinguish between intergroup and intragroup modal coupling, considering, as defined in this paper, a group of modes as the degenerate modes related to an asymmetric spatial profile LP_{lm}, $l \neq 0$. This distinction leads, firstly, into the definition of a 4×4 matrix describing the field transfer function these groups of modes $H^G(\omega)$. Secondly, it introduces a 2×2 matrix $H^{LPlm}(\omega)$ for each group of modes containing the propagation operator between the pair of degenerate modes LP_{lm}a and LP_{lm}b. Thus, the total FMF 6×6 transfer function $H_f(\omega)$, which is unitary, is constructed as

$$H_f(\omega) = \begin{bmatrix} H_{11}^G & H_{12}^G & H_{12}^G & H_{13}^G & H_{13}^G & H_{14}^G \\ H_{21}^G & H_{11}^{LP11} & H_{12}^{LP11} & H_{23}^G & H_{23}^G & H_{24}^G \\ H_{21}^G & H_{21}^{LP11} & H_{22}^{LP11} & H_{23}^G & H_{23}^G & H_{24}^G \\ H_{31}^G & H_{32}^G & H_{32}^G & H_{11}^{LP21} & H_{12}^{LP21} & H_{33}^G \\ H_{31}^G & H_{32}^G & H_{32}^G & H_{21}^{LP21} & H_{22}^{LP21} & H_{34}^G \\ H_{41}^G & H_{42}^G & H_{42}^G & H_{43}^G & H_{43}^G & H_{44}^G \end{bmatrix} \tag{25}$$

where the entries coming from H^{LP11} are framed in dashed red lines while the ones corresponding to H^{LP21} are in dashed green lines. The subindices relate to the (*row,column*) position of each entry in either H^G or H^{LPlm} submatrices.

Starting with the intergroup modal coupling, where we assume that the magnitude of Γ_p is larger than the magnitude of K_{pq} for the groups of modes p and q, and following the procedure reported in [23,24], the transfer function associated with uncoupled propagation (diagonal terms of H^G) resulting from (24) is

$$H_{pp}^G(\omega,z) = e^{-\Gamma_p(\omega)z}, \tag{26}$$

while the one related to intergroup coupling (off-diagonal terms of H^G) is

$$H_{pq}^G(\omega) = \hat{K}_{pq}\left[\int_0^z f(z')dz'\right]\Phi_{pq}(\omega,z),\ p \neq q, \tag{27}$$

where

$$\Phi_{pq}(\omega,z) = \frac{H_{pp}^G(\omega) - H_{qq}^G(\omega)}{(\Gamma_q - \Gamma_p)z} = je^{-\frac{(\Gamma_p+\Gamma_q)z}{2}}\operatorname{sinc}\left[\frac{(\Gamma_p - \Gamma_q)z}{2}\right]. \tag{28}$$

On the other hand, the matrix operator describing intragroup modal propagation and coupling is calculated as the product

$$H^{LPlm} = VH_U^{LPlm}U^*, \tag{29}$$

where H_U^{LPlm} accounts for uncoupled modal propagation:

$$H_U^{LP11} = \begin{bmatrix} H_{22}^G & 0 \\ 0 & H_{22}^G \end{bmatrix} \text{ and } H_U^{LP21} = \begin{bmatrix} H_{33}^G & 0 \\ 0 & H_{33}^G \end{bmatrix}, \tag{30}$$

while U and V are frequency-independent unitary matrices that represent the strong random coupling between degenerate modes, respectively at the input and output of the FMF, and * denotes Hermitian transpose.

Simulation of the uncoupled propagation effects was performed using a custom numerical mode solver for the calculation of the spatial profiles of the LP_{lm} modes, as well as their respective modal propagation constants $\beta_\mu{}^0$ and modal delays τ_μ calculated around the central optical wavelength λ_0 as:

$$\tau_\mu = \beta_\mu^1 = \left.\frac{d\beta_\mu(\omega)}{d\omega}\right|_{\omega_0} = -\left.\frac{d\beta_\mu(\lambda)}{d\lambda}\right|_{\lambda_0}\frac{\lambda_0^2}{2\pi c} = -\frac{\beta_\mu(\lambda_0+\Delta\lambda) - \beta_\mu(\lambda_0-\Delta\lambda)}{2\Delta\lambda}\frac{\lambda_0^2}{2\pi c} \tag{31}$$

for λ_0 = 1550 nm and $\Delta\lambda$ = 1 pm. Simulated propagation constants and modal delays are plotted in Fig. 11 for every group of degenerate modes propagating through the FMF.

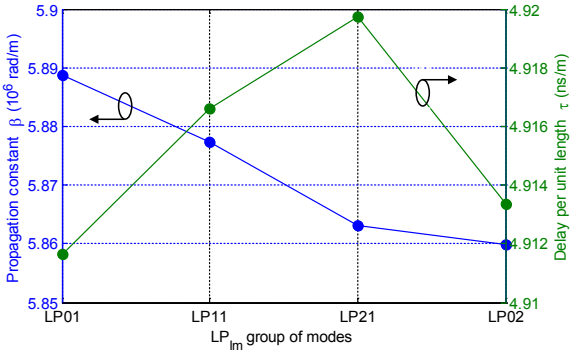

Fig. 11. Propagation constant β^0 and modal delay τ per unit length for every group of degenerate modes propagated through the selected FMF.

The attenuation α_p related to the p-th group of modes is calculated from the empirical formula proposed by Yabre for the conventional mechanisms that are present in typical fibers, i.e., absorption, Rayleigh scattering and loss on reflection at the core-cladding interface [26]. We have assumed a chromatic dispersion parameter D = 17 ps/km·nm for every mode, which leads to $\beta_\mu^2 \approx \beta_0^2$ = -21.668 ps^2/km.

The determination of the coupling coefficient K_{pq} between two guided groups of modes is achieved assuming slight core-cladding boundary imperfections at a position r as defined in [27]: $r = a_1 + f(z)\cos(m\phi)$. This formula accounts for several core boundary distortions depending on the parameter m: random core radius fluctuations for m = 0, microbends of the fiber axis for m = 1 and circular-to-elliptical deformations for m = 2. The overlap integral of the involved modes over the FMF area yields [27]:

$$\hat{K}_{pq} = -jA_{pqm}\frac{\kappa_p \kappa_q}{2n_{co,1}ka_1}, \tag{32}$$

where $\kappa_p^2 = (n_{co,1}k)^2 - \beta_p^2$ and k is the wave-number. The coefficient A_{pqm} depends on the parameter m and the pairs of groups of modes involved, assuming the values:

$$A_{pqm} = \begin{cases} 1/2 & \text{between } [\text{LP}_{01} \text{ and } \text{LP}_{02}] \\ 1 & \text{between } [\text{LP}_{11} \text{ and } \text{LP}_{21}] \\ 1/\sqrt{2} & \text{between the rest of pairs} \end{cases}. \tag{33}$$

It is necessary to determine the random core distortion function $f(z)$ to permit evaluation of (26). Both $f(z)$ and its power spectrum $< |F(\beta_p-\beta_q)|^2 >$, which is usually employed for solving the power coupling coefficient d_{pq} in power coupling models [26-28], are unknown for most practical situations. Different statistical models have been assumed depending on the autocorrelation function R_f (z_1-z_2) of $f(z)$, that is conventionally described as [27,29]:

$$R_f(z_1 - z_2) = \left\langle f_1^*(z_1) f_2(z_2) \right\rangle = \sigma^2 e^{-|z_1 - z_2|/D}, \tag{34}$$

where the autocorrelation or coupling length D is the distance at which R_f (z_1-z_2) has decreased to a fraction 1/e of its maximum value and σ^2 is the variance of $f(z)$.

The optical intensity at the output of the FMF link is computed from the ensemble average

$$P = \left\langle \tilde{E}_{FMF}^*(\omega, z)\tilde{E}_{FMF}(\omega, z) \right\rangle. \tag{35}$$

If we assume, owing to the finite correlation length D, that the field $\tilde{E}_{FMF}(\omega,z)$ and the function $f(z)$ are uncorrelated for $z >> D$ and, in addition, that $< f(z) > = 0$, from (27) and (34), we have that the contribution of optical intensity P obtained from (35) due to coupling between groups of modes becomes proportional to a parameter g^2 defined as [23]:

$$g^2 = \int_0^z \int_0^z R_f(z_1 - z_2) dz_1 dz_2 = 2\int_0^z (z - z_1) R_f(z_1) dz_1, \tag{36}$$

which is computed using (34) for $D = 4a_1 \cdot 10^4$ and σ = 1 μm.

We now have all the components needed to construct the field transfer function of the FMF according to (25). In Fig. 12, we show the modulus of $H_f(\omega)$ for a random realization of the 1-km FMF link. Each one of the six subfigures correspond to a different row of $H_f(\omega)$. First of all, one can confirm that a low level of intergroup coupling occurs, which strongly depends on the difference between the group propagation constants. The maximum value of intergroup crosstalk ranges from -45 dB affecting the LP_{01} mode to the worst case of -25 dB occurring, similarly to the designed multiplexer and demultiplexer, between the group of modes LP_{21} and the mode LP_{02}. Since Fig. 12 illustrates a random realization where we have assumed total random intragroup coupling, the entries relating each pair of degenerate modes are uniformly distributed. In this particular case, the degenerate LP_{11a} mode would receive more energy from its counterpart LP_{11b} mode (-5.9 dB) than from itself (-1.5 dB); while the interchange of energy between the degenerate LP_{21a} and LP_{21b} modes is close to the 50% (-3.4 dB and -2.8 dB). Moreover, the diagonal terms of the field transfer function $H_f(\omega)$ have modulus nearly independent of frequency, as expected if we take the modulus from (26). For modeling MGDM data transmission below, we must take into account the well-known carrier suppression effect (CSE) caused by the chromatic dispersion in direct-detection links. The spectrum of the transmitted digital signals must be placed below the first null that the CSE produces in the intensity-to-intensity transfer function of a dispersive link. This null occurs at a frequency $f_1 = 1/(2\sqrt{\pi\beta_0^2 L})$ = 60 GHz for a link length L = 1 km and a chirp-free modulated signal.

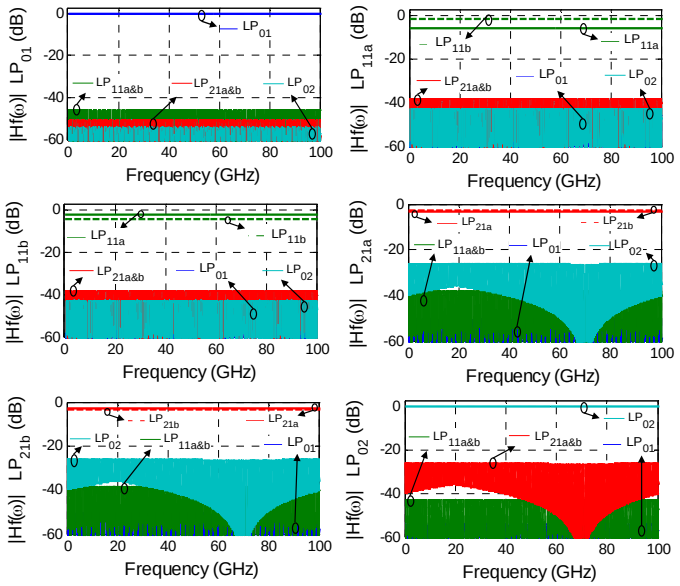

Fig. 12. Modulus of the field transfer function of the 1-km FMF link, $|H_f(\omega)|$.

It is worth recalling that we employ a propagation model based on linearly polarized modes LP_{lm}, an approximation valid for weakly guiding fibers characterized by a normalized index difference $\Delta<<1$, [30]. The LP_{lm} pseudomodes actually comprise one (for $l = 0$) or two (for $l \neq 0$) true modes (HE, EH, TE and TM modes), which have slightly different propagation constants that can be computed from the exact modal theory.

Our MGDM systems transmits data channels 2 and 3 through the groups of asymmetric LP_{lm} modes ($l \neq 0$). Within each group, the propagation of the degenerate LP_{lma} and LP_{lmb} modes has been modeled assuming strong random coupling between them, as described by (29). Referring to the exact modal theory, both LP_{11a} and LP_{11b} are actually a superposition of the TE_{01} and HE_{21} or TM_{01} and HE_{21} true modes, while both LP_{21a} and LP_{21b} are a superposition of the HE_{31} and EH_{21} true modes. In order to assure a proper recovery of the data channels transmitted through channels 2 and 3, it is desirable to have negligible intramodal dispersion effects in each pair of true modes. This phenomenon, also referred as modal birefringence [31], arises from the slight difference in the propagation constants of the two constituent true modes and is further affected by the strong coupling caused between them, [32]. The difference in the group velocity ($\Delta\beta^1_{LPlm}$) and the difference in the propagation constants ($\Delta\beta^0_{LPlm}$) between two nearly degenerate true modes can be computed from the modal birefringence function $B(v)$, [31]. For the FMF employed in our transmission system, we obtained $\Delta\beta^0_{LP11}$ = 8.06 rad/m for the pair (TE_{01},HE_{21}) and -1.39 rad/m for the pair (TM_{01},HE_{21}), and $\Delta\beta^0_{LP21}$ = 10.59 rad/m; while $\Delta\beta^1_{LP11}$ = 19.89 fs/m for the pair (TE_{01},HE_{21}) and -3.31 fs/m for the pair (TM_{01},HE_{21}), and $\Delta\beta^1_{LP21}$ = 26.12 fs/m. We expect that the typical perturbations that break the fiber symmetry will cause strong random coupling between the two constituent true modes. The sources of this degenerate modal coupling include polarization birefringence, bending, twist, core ellipticity and Faraday rotation of polarization [32]. As deduced from modal coupling theory, strong coupling mitigates the modal dispersion, preventing it from accumulating linearly with the fiber length L [34]. As a consequence, we assume that the dispersion potentially arising from the group velocity differences ($\Delta\beta^1_{LPlm}$) described above, will be rendered negligible.

IV. End-To-End Data Link

The performance evaluation of the end-to-end MGDM system, comprising the designed multiplexer and demultiplexer and the selected 1-km FMF link is performed considering efficiency (optical losses) and inter-channel crosstalk criteria. The design characteristics of the multiplexer and demultiplexer were specified in Section II, while the FMF characteristics were described in Section III. We assume that the diversity combining required for the asymmetric LP_{lm} modes is implemented by the optical combining method described in section II.C, which adaptively co-phases the optical signal in the SMF outputs before combining them in a 3-dB coupler, [22]. Alternatively, diversity combining could be implemented with any of the three electrical diversity combining techniques (BSC, EGC and MRC) discussed in Section II.C. The MGDM system is as shown in Fig. 1 for N = 4 data channels and M = 6 propagating spatial modes. One of the advantages of the developed model lies in the ability of designing and characterizing the overall optical link, as depicted in Fig. 1, using the field transfer function $H(\omega)$

$$\tilde{E}_{out}(\omega) = H(\omega)\tilde{E}_{in}(\omega), \qquad (37)$$

which is represented as the product of the matrices representing the field transfer function of the demultiplexer (14), the fiber (25) and the multiplexer (13), i.e., $H(\omega) = H_{DEMUX}(\omega)\, H_f(\omega)\, H_{MUX}(\omega)$. The behavior of the multiplexer, demultiplexer and FMF have been respectively characterized in Figs. 7, 9, and 12. The modulus of the total transfer function for each element of the matrix $H(\omega)$, i.e., for each pair output-input channel, is shown in Fig. 13 for the same random realization that characterized the FMF intermodal coupling response in Fig. 12. We see that approximately no loss (less than 1 dB) can be guaranteed for every channel output. The maximum crosstalk level is kept around -25 dB for the first two channels, while it increases up to -15 and -18 dB for the third and fourth channels, as expected from the crosstalk evaluation in Sections II and III. The end-to-end data transmission evaluation will determine if these crosstalk levels, a consequence of having considered the LP_{21} and the LP_{02} mode groups as independent transmission channels, excessively degrade system performance.

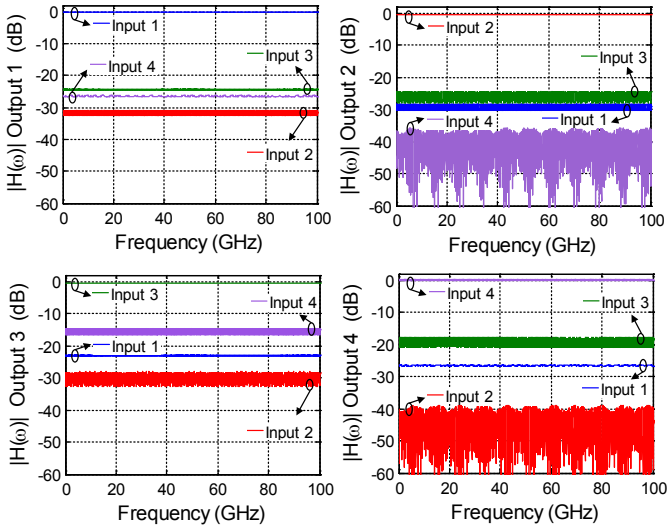

Fig. 13. Modulus of the field transfer function of the total optical link, $|H(\omega)|$.

We use these four groups of modes to transmit four different digital data signals modulated using on-off keying (OOK) at a bit rate of 32 Gb/s. These electrical data streams, composed of 1023-symbol sequences (N_{prbs} = 10), externally modulate four independent lasers emitting 0 dBm at a wavelength centered at 1550 nm through four identical electro-optic modulators. The modulated signals are considered chirp-free. We assume the use of four independent lasers, instead of a single common laser, so incoherent crosstalk occurs between the four channels, since the relative optical phases between the desired and the interference signals vary randomly on a time scale comparable to the coherence time of the optical source. To take into account this condition we added a random phase, uniformly distributed in the range $[0,2\pi]$, to the optical field at the output of each external modulator, $\tilde{E}_{in}(t)$. After mode-group multiplexing, transmission through the 1-km FMF link and mode-group demultiplexing, the signals are photodetected (photodiode responsivity R = 1 A/W), filtered by a five-pole Bessel lowpass filter, and sampled. Since no optical inline amplifiers are included, this MGDM system is thermal noise-limited. Independent but identically distributed thermal noise sources (noise figure NF = 3 dB over a load resistor of 50 Ω at a room temperature of 300 K) have been considered for each received channel. Fig. 14 shows the recovered eye diagrams (output voltage $Vout_i$) for all four received channels for a random system realization. Although a small amount of crosstalk can be observed between the received data channels 3 and 4, following the trend already discussed for the multiplexer, fiber and demultiplexer, the figure clearly shows open eye diagrams for every detected channel.

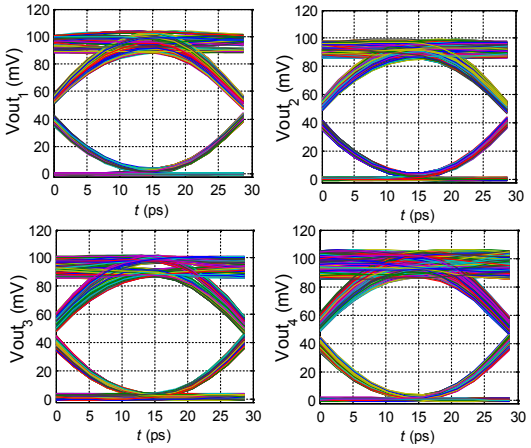

Fig. 14. Recovered eye diagrams for each channel output.

The evaluated figures of merit, quality factor Q and bit-error ratio (BER), are represented as the average of 20 random realizations accounting, as indicated before, the random phase of the input optical field $\tilde{E}_{in}(t)$ as well as the random intragroup and intergroup modal coupling. Fig. 15 shows the simulated quality factor Q in dB, as a measure of the signal to noise ratio, when varying the optical power before photodetection over a 24-dB range. Since our case implies OOK modulation and direct detection, the plotted quality factor has been computed as $Q = (I_1-I_0)/(\sigma_0+\sigma_1)$, assuming transmission of ones and zeros with equal probability for probability density functions (output voltage) that can be well approximated by Gaussian functions with respective means I_1, I_0 and standard deviations σ_0 and σ_1. In order to estimate the signal to noise ratio penalty introduced by the MGDM system, we added in Fig. 15 the calculated Q curve (black line) for the transmission of one 32-Gb/s OOK-modulated data channel through 1-km SMF link accounting for optical loss (0.25 dB/km) and chromatic dispersion (D = 17 ps/km·nm). We can observe, on the one hand, that channels 1 and 2 follow a similar tendency, gradually reaching a respective plateau of approximate 24.5 and 25.6 dB for optical attenuation levels lower than 10 dB. On the other hand, the Q^2 factors of channels 3 and 4 reach a lower plateau level of approximate 15.9 dB and 18.8 dB, respectively. These values are in concordance with the pertinent interchannel crosstalk levels deduced from the link transfer function shown in Fig. 13. All in all, a maximum 9.7-dB variation is observed between the received data channels. In comparison to the SMF link performance, a maximum MGDM system penalty ranging from 10.4 dB (Channel 2) up to 20.20 dB (Channel 3) is reached when no attenuation is applied. Quality factor values above 15 dB are experienced for attenuation levels approximately lower than 13.5 dB for output channels 1 and 2, while for attenuation values lower than 6 and 11.5 dB, respectively, for channels 3 and 4. This Q^2 figure corresponds approximately to an expected BER below 10^{-9}, as depicted in Fig. 16.

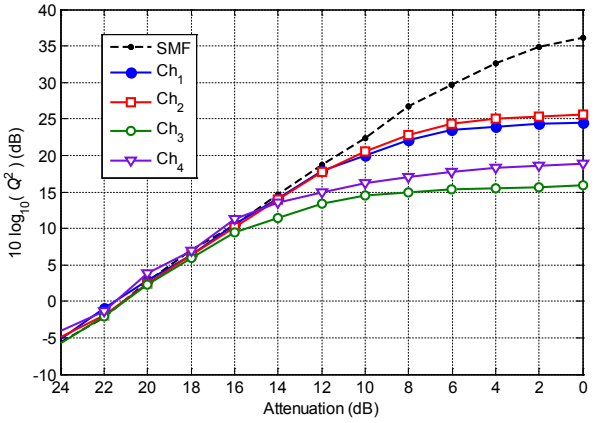

Fig. 15. Quality factor Q in dB for each recovered channel.

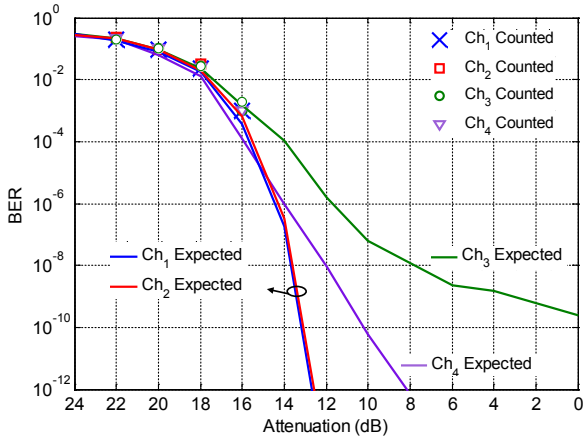

Fig. 16. Expected and counted bit-error ratio for each recovered channel.

We have distinguished between the so-called *measured* or *counted BER*, $BER|_{count}$, calculated as the ratio between the number of counted bit errors and the number of transmitted bits and plotted as markers, and the estimated or *expected BER* calculated from the Q factor through $BER|_{exp} = ½\ erfc\ (Q/\sqrt{2})$ and plotted in solid lines. In line with the computed Q^2 results, similar values of the estimated BER are obtained for channels 1 and 2. The expected BER curve for channel 3 shows some degradation for attenuation levels lower than 14 dB, reaching a minimum expected BER of approximate $2 \cdot 10^{-10}$. It must be noted that actually no error was counted for attenuation levels below 16 dB. The computed averaged values of Q and BER assure in consequence an error-free transmission for the direct-detection MGDM link designed with multiplexer /demultiplexer devices based on few-core selective modal couplers.

V. Conclusions

In view of the performance evaluation carried out for the addressed end-to-end MGDM direct-detection system, we conclude that the designed fiber-based multiplexing and demultiplexing technology, built over few-core selective couplers matched to individual groups of degenerate modes, makes feasible error-free MGDM transmission. Since this approach is based on direct detection, it avoids the use of the digital signal processing required for MIMO demultiplexing in coherent-detection systems, which have, to date, the predominant approach for SDM over FMFs. The range of application of our approach is in consequence subject to short-reach scenarios where intergroup coupling can be kept to a relative low level, such as converged fiber-wireless radio access networks, fiber-to-the-home distribution architectures or dense interconnect networks in data centers. We envision that the described mode-selective couplers can, in addition, serve as a lossless solution for a selective modal switch where a specific channel is required to be added or extracted.

References

[1] T. Morioka, M. Jinno, H. Takara, and H. Kubota, "Innovative Future Optical Transport Network Technologies," *NTT Review*, vol. 9, no. 8, pp. 1-8, 2011.

[2] D. J. Richardson, J. M. Fini, and L. E. Nelson, "Space-division multiplexing in optical fibers", *Nat. Phot.*, vol. 7, pp. 354-362, 2013.

[3] H. R. Stuart, "Dispersive multiplexing in multimode optical fiber," *Science*, vol. 289, pp. 281-283, 2000.

[4] S. Randel et al., "6×56-Gb/s mode-division multiplexed transmission over 33-km few-mode fiber enabled by 6×6 MIMO equalization," *Opt. Expr.*, vol. 19, no. 17, pp. 16697-16707, 2011.

[5] C. Koebele et al., "Two mode transmission at 2x100Gb/s, over 40km-long prototype few-mode fiber, using LCOS-based programmable mode multiplexer and demultiplexer," *Opt. Expr.*, vol. 19, no.17, pp. 16593-16600, 2011.

[6] R. Ryf et al., "12x12 MIMO Transmission over 130-km Few-Mode Fiber," in Proc. of Frontiers in Optics, p. FW6C4, Rochester, USA, Oct. 2012.

[7] M. Salsi et al., "Mode-Division Multiplexing of 2x100 Gb/s Channels Using an LCOS-Based Spatial Modulator," *IEEE J. Lightw. Technol.*, vol. 30, no.4 pp. 618-623, 2012.

[8] J. Carpenter and T. D. Wilkinson, "All optical degenerate mode-group multiplexing using a Mode Selective Switch," in Proc. of IEEE Phot. Society Summer Topical Meet., pp. 236-237, Seattle, USA, July 2012.

[9] R. A. Panicker, J. P. Wilde, J. M. Kahn, D. F. Welch, and I. Lyubomirsky, "10x10Gb/s DWDM Transmission Through 2.2km Multimode Fiber Using Adaptive Optics," *IEEE Photon. Technol. Lett.*, vol. 19, no. 15, pp. 154-1156, 2007.

[10] R. Ryf, N. K. Fontaine, and R. Essiambre, "Spot-based mode coupler for mode-multiplexed transmission in few-mode fiber'', in Proc. of IEEE Phot. Society Summer Topical Meet., pp. 199-200, Seattle, USA, July 2012.

[11] A. Al Amin, A. Li, S. Chen, X. Chen, G. Gao, and W. Shieh, "Dual-LP11 mode 4x4 MIMO-OFDM transmission over a two-mode fiber," *Opt. Expr.*, vol. 19, no. 17, pp. 16672-16679, 2011.

[12] J. D. Love and N. Riesen, "Mode-selective couplers for few-mode optical fiber networks," *Opt. Lett.*, vol. 37, no. 19, pp. 3990-3992, 2012.

[13] N. Riesen and J. D. Love, "Weakly-Guiding Mode-Selective Fiber Couplers," *IEEE J. of Quantum Electron.*, vol. 48, no. 7, pp. 941-945, 2012.

[14] N. Riesen and J. D. Love, "Few-core Spatial-mode multiplexer/ demultiplexer based on evanescent coupling," *IEEE Photon. Technol. Lett.*, vol. 25, no. 14, pp. 1324-1327, 2013.

[15] N. K. Fontaine, R. Ryf, J. Bland-Hawthorn, and S. G. Leon-Saval, "Geometric requirements for photonic lanterns in space division multiplexing;" *Opt. Exp.*, vol. 20, no. 24, pp. 27123-27132 ,2012.

[16] N. K. Fontaine, S. G. Leon-Saval, R. Ryf, J. R. Salazar Gil, B. Ercan, and J. Bland-Hawthorn, "Mode-Selective Dissimilar Fiber Photonic-Lantern Spatial Multiplexers for Few-Mode Fiber," in Proc. ECOC, paper PD1.C.3, London, UK, 2013

[17] C. R. Doerr, "Silicon photonics for space-division multiplexing," presented at IEEE Photonics Society Summer Topical Meeting, pp. 242-243, July 2012.

[18] A. M. J. Koonen, H.-S. Chen, H. P. A. van den Boom, and O. Raz, "Silicon Photonic Integrated Mode Multiplexer," presented at IEEE Photonics Society Summer Topical Meeting, pp. 240-241, 2012.

[19] A. Yariv, "Coupled-mode theory for guided-wave optics," *IEEE J. of Quantum Electron.*, vol. QE-9, no. 9, pp. 919-933, 1973.

[20] N. Riesen and J. D. Love, "Ultra-broadband tapered mode-selective couplers for few-mode optical fiber networks," *IEEE Photon. Technol. Lett.*, vol. 25, no. 24, pp. 2501-2504, 2013.

[21] A. Goldsmith, "Diversity," in *Wireless Communications*, Cambridge University Press, 2005.

[22] C. R. Doerr, "Proposed Architecture for MIMO Optical Demultiplexing Using Photonic Integration," *IEEE Photon. Technol. Lett.*, vol. 23, no. 21, pp. 1573-1575, 2011.

[24] I. Gasulla and J. Capmany, "Transfer function of multimode fiber links using an electric field propagation model: Application to Radio over Fibre Systems," *Opt. Expr.*, vol. 14, no. 20, pp. 9051-9070, 2006.

[25] B. E. A. Saleh and R. M. Abdula, "Optical Interference and Pulse Propagation in Multimode Fibers," *Fiber Integr. Opt*., vol. 5, no. 2, pp. 161-201, 1985.

[26] D. Gloge, "Optical Power Flow in Multimode Fibers," *Bell Syst. Tech. J.*, vol. 51, no. 8, pp. 1767-1783, 1972.

[27] G. Yabre, "Comprehensive Theory of Dispersion in Graded-Index Optical Fibers," *IEEE J. Lightw. Technol.,* vol. 18, no. 2, pp. 166-177, 2000.

[28] D. Marcuse, Theory of Dielectric Optical Waveguide, Academic Press, 2nd edition, 1991.

[29] R. Olshansky, "Mode Coupling Effects in graded-index core fibers," *Appl. Opt.*, vol. 14, no. 4, pp. 935-945, 1975.

[30] C. Antonelli, A. Mecozzi, M. Shtaif, and P. J. Winzer, "Random coupling between groups of degenerate fiber modes in mode multiplexed transmission," *Opt. Expr.*, vol. 21, no. 8, pp. 9484-9490, 2013.

[31] D. Gloge, "Weakly Guiding Fibers," *Applied Optics*, vol. 10, no. 10, pp. 2252-2258, 1971.

[32] H. Kogelnik and P. J. Winzer, "Modal Birefringence in Weakly Guiding Fibers," *IEEE J. of Lightw. Technol*., vol. 30, no. 14, pp. 2240-2245, 2012.

[33] L. Palmieri and A. Galtarossa, "Coupling Effects Among Degenerate Modes in Multimode Optical Fibers," *IEEE Photon. J.,* vol. 6, no. 6, pp. 1-8, 2014

[34] K.-P. Ho, and J. M. Kahn, "Statistics of Group Delays in Multimode Fiber With Strong Mode Coupling," *IEEE J. of Lightw. Technol*., vol. 29, no. 21, pp. 3119-3128, 2011.